Physics 6268
Website: invertpend.wordpress.com

# Stabilization of an inverted pendulum via periodic forcing

Samuel A. Shapero*, Yiwei Chang, Robert Hayward
*Primary Author, samshap@gatech.edu *Department of Electrical and Computer Engineering, Georgia Institute of Technology*

## Abstract

We reconstruct a model for an inverted pendulum with periodic vertical forcing. By integrating with a ODE solver in MATLAB, we calculate the regions of stability for the pendulum. We hypothesize that modifying the vertical perturbation to a Jacobi Elliptic function will increase the region of stability, and verify with initial simulations. An inverted pendulum is mounted to a shaker table, perturbed with periodic, controlled accelerations. Displacement is tracked via a high speed camera, and used to determine natural frequency and damping. We modify the model to remedy discrepancies between numerical and experimental data. A precise relationship between frequency and amplitude emerges at the boundary of stability, and we create an original analytical derivation that explains it. We conclude that for similar displacement and frequency, modifying the eccentricity of the Jacobi Elliptic function has no effect.

**Keywords:** Inverted Pendulum, Periodic Forcing, Stability, Jacobi Elliptic

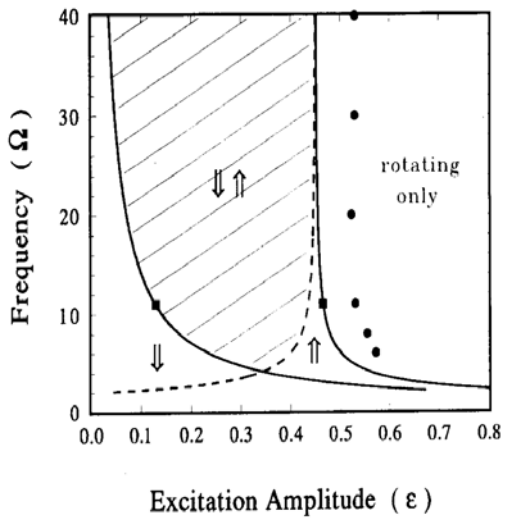


**Figure 1**. Stability diagram for a vertically forced pendulum [1], as a function of relative frequency and relative amplitude of the forcing oscillation. The up arrow indicates stability for an inverted pendulum, while the down arrow indicates stability for a non-inverted pendulum. High amplitude vibrations will only result in rotation.

## 1. Introduction

The pendulum has long been an object of fascination and great import to physicists, as it represents the basic building block of any rotating system in a constant gravitational field. It also has many dynamical properties of interest to the mathematician. Under different forcing conditions, a pendulum may approach a stable fixed point, may oscillate, rotate around its axis, or even behave chaotically.

The inverted pendulum is a special case where the pendulum's center of mass is stabilized above the axis of rotation. Inverted pendulums occur in civil engineering wherever a tall structure, such as a crane [2], needs to be balanced. In biomechanics, balance in bipeds is modeled by an inverted-pendulum, and artificial control for stability could be used to compensate for the natural loss of balance that occurs with age [6,7].

Our primary objective was to investigate the theoretical model of the vertically forced inverted pendulum, and to determine its regions of

stability. We hypothesized that modifying the forcing function to have high order harmonics would increase the region of stability. We sought to test this hypothesis numerically and empirically.

## 2. Model and Literature Review

Forced pendulums have been studied extensively, and their attractors and bifurcations have been extracted by mathematical analysis [4,5], computer simulation [1,3], and physical experimentation [10]. It is well established that the inverted pendulum can be stabilized under high frequency vertical vibrations. Blackburn et al. [1], and Smith et al. [10] investigated the vibration parameters necessary for stabilization.

The vertically, periodically forced inverted pendulum can be modeled as

$$I\ddot{\theta} + \beta\dot{\theta} - Mrg\sin(\theta) = F(\omega t')\sin(\theta) \quad (1),$$

where $\theta$ is the angle from the apex, $I$ is the pendulum's moment of inertia, $\beta$ is the damping coefficient, and $F(\omega t)$ is a periodically applied force with frequency $\omega$. By setting $t = \omega t'$ and defining $\omega_0^2 = Mrg/I$ as the natural frequency of the pendulum, we can rewrite (1) as

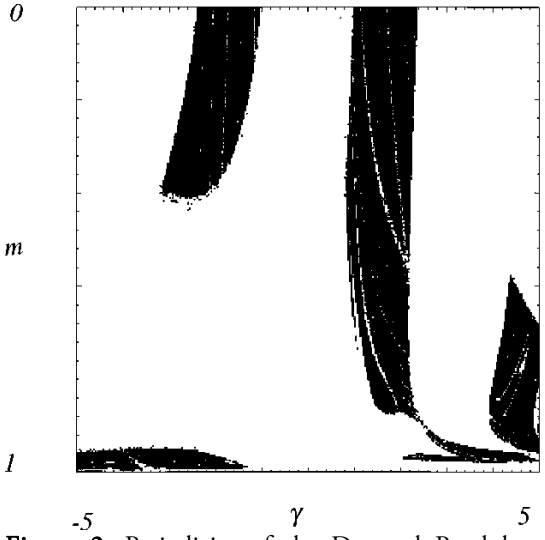


**Figure 2**. Periodicity of the Damped Pendulum with Jacobi Elliptical forcing [9]. 0<m<1 determines the shape of the forcing waveform, and γ is the relative amplitude of that perturbation. Negative γ indicate inverted operation. Black regions indicate chaos, white regions periodic or stable behavior.

$$\ddot{\theta} + \frac{\beta}{I\omega}\dot{\theta} - \left(\frac{\omega_0^2}{\omega^2} - F(t)\right)\sin(\theta) = 0 \quad (2).$$

Blackburn et al. used a sinusoidal forcing function

$$F(t) = a/r_* \cos(t) \quad (3),$$

where $a$ is the amplitude of the externally applied oscillations, and $r^*=I/Mr$. Blackburn et al. calculated the regions of stability while varying $\Omega = \omega/\omega_0$, and $\varepsilon = a/r*$, the normalized frequency and amplitude (Figure 1). Their analysis, however, used simplifying assumptions that reduced (2) to a linear equation.

Levi et al. [4] went a step further, proposing parabolic oscillations. These permitted completely linear behavior for each cycle, allowing for an intuitive proof of stability for certain frequencies. Sanjuan [8,9] noted that the true dynamics of the pendulum are nonlinear, corresponding to Jacobi Elliptical trajectories in phase space (see Appendix A). Thus they decided to use the Jacobi Elliptical function *cn* as a forcing function:

$$F(t) = a/r\, cn(t, m) \quad (4)$$

They found that varying the eccentricity factor $m$ in the Jacobi Elliptical function could lead to bifurcations in the periodicity of the damped pendulum (Figure 2). This degree of freedom would allow a user to choose between periodic, quasi-periodic, and chaotic dynamics even when the relative amplitude and frequency of the external force were fixed.

## 3. Methods

### *3.1 Numerical Simulations*

We first decided to simulate the inverted pendulum (2) with forcing equation (4). We varied three parameters in our simulations: the Jacobi Elliptic factor $m$, varied between 0 and 1; the relative amplitude ε, which ranged up to .5; and the relative frequency, which ranged up to 100. The relative drag $\frac{\beta}{I\omega}$ was set to a constant 0.1 to have only a minor effect on the dynamics, while still providing damping.

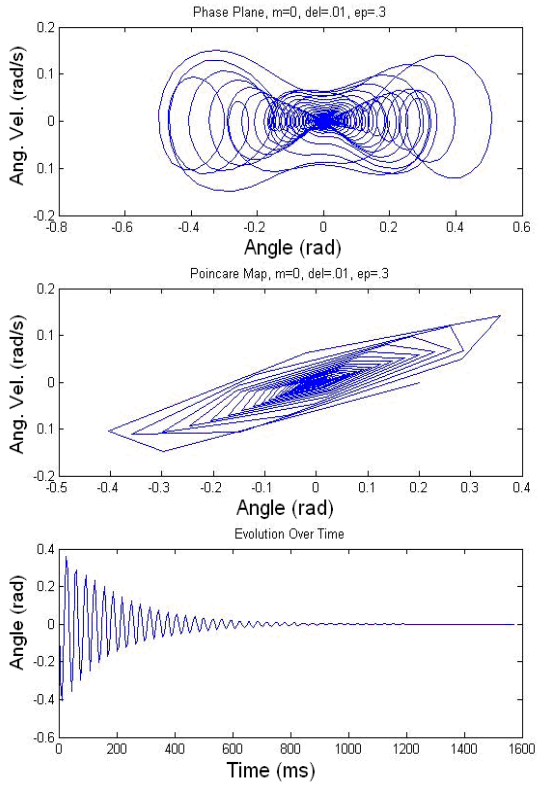


**Figure 3**. Stable dynamics in the phase plane for the inverted pendulum with sinusoidal forcing. Pendulum is upright when $\theta = 0$. Since the system is actually three dimensional, a two dimensional mapping onto the phase plane (top) is hard to read. By sampling every period (middle) we can show the evolution of the Poincare map in the phase plane. We also include the temporal dynamics (bottom).

Simulations were performed in Matlab, using the 4th order Runge-Kutta ODE solver, ode45. Our model was fundamentally a third order system, with $t$, $\theta$ and $\dot{\theta}$ as distinct independent variables. Since the effect of t was periodic, we created a two-dimensional Poincaré map by sampling $\theta$ and $\dot{\theta}$ once every period, where

$$P_n = \left(\theta(nT), \dot{\theta}(nT)\right) \quad (5),$$

and T was the period of the Jacobi Elliptic function (see Appendix A).

Figure 3 illustrates the trajectory of a pendulum with sinusoidal forcing, initial position 0.2 radians from center, and initial angular velocity of 0 rad/s. The Poincaré map and temporal dynamics are shown to make the dynamics more clear.

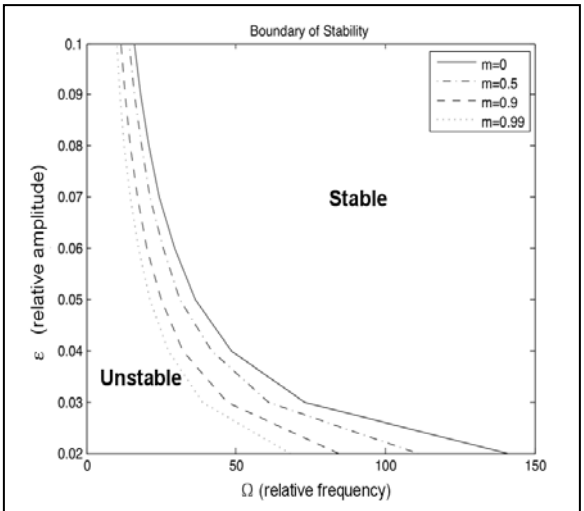


**Figure 4.** Boundary of stability for inverted pendulum with Jacobi Elliptic forcing. For each value of m, the stable region is above the curve. This preliminary model shows that increasing the eccentricity $m$ of the forcing function enlarges the region of stability.

In order to find the boundaries of the region of stability (as in Figure 1), we simulated the trajectory at a variety of eccentricity and relative frequency values. At each node of eccentricity and frequency, we performed a binary search of relative amplitudes, allowing us to zoom in on the stability boundary. Figure 4 shows the region of stability we calculated, and demonstrates that, for our given modeling assumptions, a more eccentric forcing function will produce a larger region of stability.

### *3.2 Experimental Setup*

In order to verify the accuracy of our Matlab simulations, we set up an inverted pendulum arm on a shaker table with controllable acceleration. Figure 5 illustrates the setup, including a block diagram showing the method of control and observation. The shaker table was attached to a magnetic actuator that converted an electrical signal into mechanical force, similar to a speaker.

An ADXL321 accelerometer was mounted to the underside of the shaker, in order to monitor the acceleration for feedback and recording. A signal of 50mV per g of acceleration was sent to a computer with a Labview testbench that

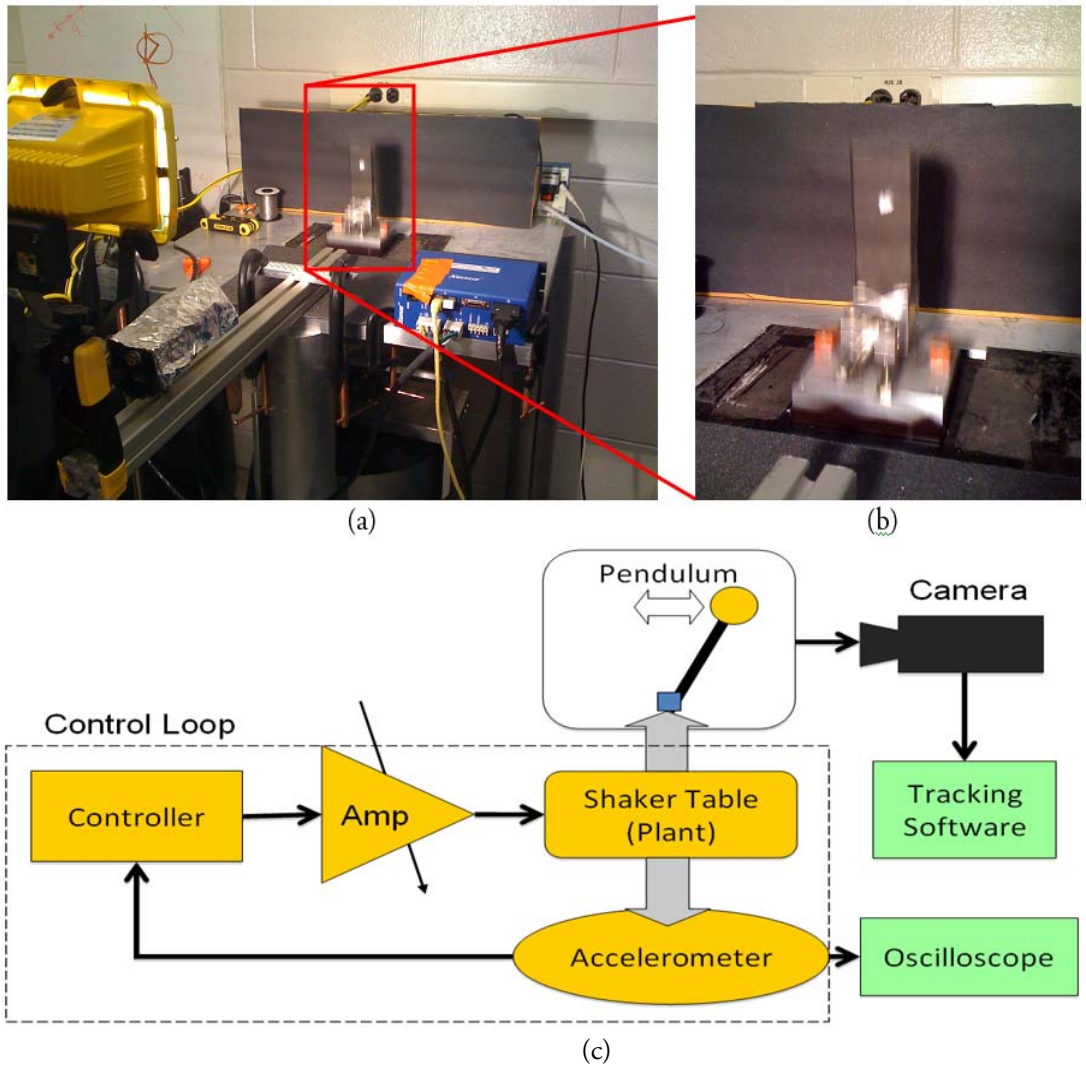


**Figure 5** Apparatus for controlling inverted pendulum. (a) The shaker table, with the signal input, accelerometer output, and inverted pendulum mounted on top. A camera is mounted in front, and tracks the white spot painted on the pendulum. A light is projected on the pendulum to help the spot stand out. (b) A close up of the pendulum, mounted on the shaker. Bumpers were added to restrict the range of motion. (c) Block diagram of the control scheme. A software controller implemented in Labview outputs the desired waveform, based on feedback from the accelerometer. The waveform is amplified by an VTS-500 high powered amplifier and sent to the shaker table. The acceleration from the shaker table is transmitted to the sensor, an ADXL321 accelerometer, which feeds back to the controller, and to an oscilloscope (acting as a sanity check for the amplitude of accelerations). The acceleration is also transmitted to the fulcrum of the inverted pendulum, causing the desired dynamic equation. A high speed camera observes the motion of the pendulum and sends the video to a second Labview testbench, which records the x and y position of the white spot.

controlled the waveform. The software controlled the amplitude of each harmonic component separately, permitting a wide range of waveforms, including Jacobi Elliptics of varying eccentricity. This signal was then broadcast to an VTS-500 high powered amplifier, which boosted the signal to the level necessary for the shaker. Acceleration data was also sent to an oscilloscope, from which the peak acceleration could be monitored independently of the controller.

During our experiments we had some trouble with the controller, which had difficulties managing the amplitude of the signal correctly in real time. As a result, we would often first run the controller to have the right waveshape, and then disable any further change. To modulate the amplitude of acceleration, we relied on the variable gain knob of the amplifier.

The inverted pendulum itself consisted of a 3.8cm x 11.9cm aluminum arm, with a fulcrum centered 1.9cm from one end (see Figure 5b). The arm was 6.4mm (1/4") thick, except for a 3.8cm x 3.8cm square centered about the fulcrum having twice the thickness. The total mass of the arm was approximately 80g, the radius of the center of mass $r$ was 3.1cm, and its moment arm ($I/M$) was 23cm$^2$. The natural frequency of the arm $\omega_0$ was 11.5 radians per second (rad/s) and the effective radius $r^*$ was 7.4cm. For data collection purposes, the arm was covered in black paper, and a spot of white-out was centered 7.1cm from the fulcrum.

### *3.3 Data Collection*

A high speed camera was mounted directly in front of the pendulum, and took photos at up to 200 frames per second (fps). The higher speeds caused erratic frame rates, so the camera was generally operated at 100 fps. The images were sent to a second computer with a Labview tracking program. The program applied a threshold of luminance to identify the spot, and tracked the centroid of the spot within a torus section selected by the user. The program was able to track the relative x and y position of the dot, from which the angle of the pendulum could be extracted. While the pendulum was in the stable inverted position, the vertical displacement of the pendulum equaled the vertical displacement of the shaker table, and so could be used to determine the amplitude of the forcing displacement.

To determine the region of stability, we recapitulated our procedure from the numerical trials. We varied the driving frequency from 20Hz to 50Hz, and the eccentricity from 0 to 0.999. At each node, we attempted to increase the

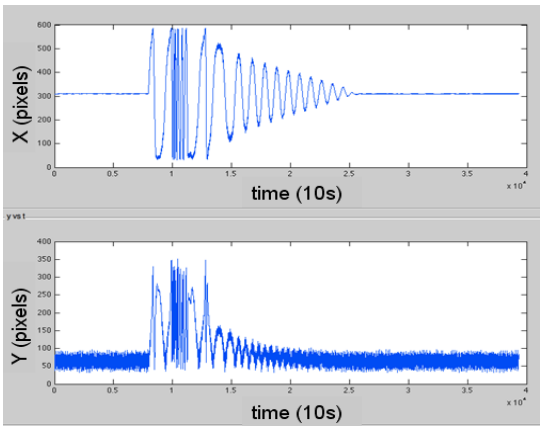


(a)

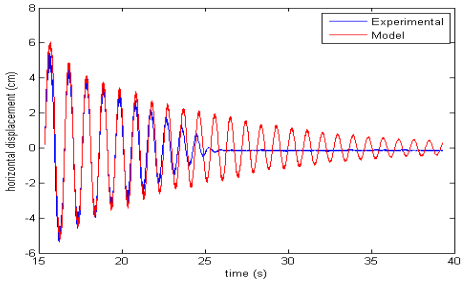


(b)

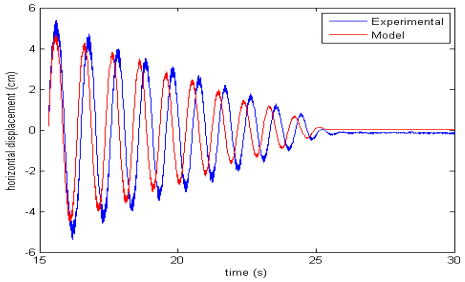


(c)

**Figure 6.** Motion of a stable inverted pendulum. (a) Experimental results. The pendulum begins stable, then at t=8s is pushed by the tester. The pendulum bounces off the bumpers until t=13s, where self-stabilizes back to the inverted positon. Residual vertical oscillation is due to the forcing function, with $m$=0.999, $f$=26Hz, p-p accel=80g. (b) Comparison of recorded horizontal displacement with initial model of inverted pendulum with linear damping. Note the exponential decay in the model. (c) Comparison of recorded horizontal displacement with improved model of damping as a frictional torque, with a relative value of .155rad/s$^2$. Note that the experimental data stabilizes off center, due to static friction, which was not included in the model.

acceleration until the inverted pendulum became stable in the upright position. For those nodes that we could stabilize, we then decreased the acceleration slowly until stability was spontaneously lost. We then returned the pendulum to stability and recorded the acceleration and the displacement of the forcing function. This process had two main sources of noise: it was difficult to fine tune the acceleration to within 1g; at the boundary of stability, it was sometimes subjective whether the pendulum was truly stable.

## 4. Results

Figure 6 illustrates a typical response of the stable inverted pendulum. We used these curves to calculate the damping coefficient and the natural frequency. Unfortunately, our initial numerical model proved a poor fit for the dynamics of the real system. Whereas the model predicted an exponential decay of oscillations around a stable fixed point, we observed an almost linear decay.

We observed several other strange behaviors that our model did not predict. Forcing accelerations close to the boundary of stability, for example, would sometimes produce a stable fixed point that was non-vertical. At other times, it would induce a chaotic wobbling behavior around the vertical position. Both of these contravened the model, which only predicted a stable fixed point at the vertical position.

The boundary of stability itself was characterized by two trends: a linear relationship between the frequency and the peak-to-peak acceleration, and an inverse relationship between peak-to-peak displacement and frequency (Figure 7). Both of these trends indicated that stability was determined by the velocity of the signal, irrespective of frequency, since, for a periodic signal $x_C(\omega t) \propto 1/\omega$, the velocity was constant:

$$\frac{d}{dt}x(\omega t) = \omega x'(\omega t) \propto \omega x \propto 1 \quad (6);$$

Matching the data, the acceleration was:

$$\frac{d^2}{dt^2}x(\omega t) = \omega^2 x''(\omega t) \propto \omega^2 x \propto \omega \quad (7).$$

Because both displacement and acceleration were limited by our system, these dependencies limited the range of stabilizable frequencies. Low

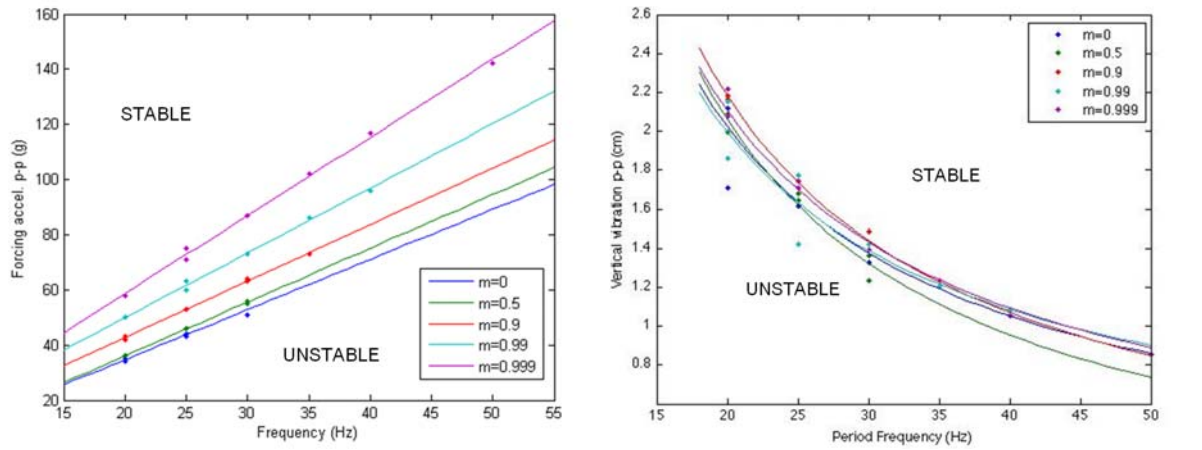


(a) (b)

**Figure 7.** Stability regions of the inverted pendulum. (a) Stability as a function of peak-to-peak acceleration of the forcing function. The data points are the minimum accelerations that stabilized the inverted pendulum, and the curves are the best linear fit. For each *m*, the region above the curve is stable, and the region below is unstable. The required acceleration for stability scales linearly with frequency, and increases monotonically with *m*, proportional to $1/s(m)$ (see Appendix B). Note that the inverted pendulum can only be stabilized at 50Hz when $m = 0.999$. (b) Stability as a function of peak-to-peak displacement. Data points are fit to the closest inverse curve. Again, only the region above the curves is stable. The required displacement scales inversely with frequency, while it appears that *m* has not effect.

frequencies would require displacement larger than the 2.6cm the shaker table would allow. High frequencies would require accelerations beyond the driving capabilities of the amplifier.

In contradiction to our original model in Figure 4, the eccentricity *m* had no noticeable effect on the displacement required to stabilize each frequency (Figure 7b). Any dependency that might have existed was confounded by our noisy measurement procedure. The eccentricity did have other effects, however; the peak acceleration required to stabilize the inverted pendulum at a given frequency rose monotonically with *m*. At the same time, the maximum achievable acceleration rose even faster with *m*. This allowed us to stabilize the pendulum at much higher frequencies for *m*=0.999 than for *m*=0 (Figure 7a). This may have been due to the power spectrum being divided between multiple harmonics for high *m.*

## 5. Discussion

### *5.1 Improving the Model*

The experimental data contradicted two important parts of our preliminary model. First the decay of oscillations around the stable fixed point indicated that our damping model was incorrect; the linear decay of the oscillations strongly suggests that damping was due to a constant torque opposite the direction of motion.

Friction at the bearing could account for the linear decay in Figure 6a, since it is independent of the angle and angular speed of the pendulum (although its sign should always be opposite the angular velocity). By replacing the drag torque in (1) with a dynamic frictional torque of magnitude *k*, our dynamical equation becomes:

$$I\ddot{\theta} + sign(\dot{\theta}) \cdot k - Mrg\sin(\theta) = F(\omega t')\sin(\theta) \quad (8).$$

And renormalizing with $t = \omega t'$, this becomes:

$$\ddot{\theta} + \frac{K}{\Omega^2} sign(\dot{\theta}) - \left(\frac{1}{\Omega^2} - F(t)\right)\sin(\theta) = 0 \quad (9),$$

where $K = k/I\omega_0^2 = k/Mrg$ and $\Omega = \omega/\omega_0$. In the special case where $\dot{\theta} = 0$, we use a static friction term that negates all forces below a threshold $F_S$. Comparing the numerical simulation with the experimental data allowed us to deduce a best fit value for K. Figure 6c shows the results of this improved mapping.

Another problem with our model was the scaling of the Jacobi Elliptical function, both in frequency and amplitude. Our original model did not account for the elongated period of the Elliptical function when $m > 0$. Additionally, we used the simplifying assumption that amplitude of displacement was $1/\omega^2$ times the amplitude of the acceleration. For $cn(t, m > 0)$, this is not the case, because it contains higher order harmonics that are attenuated by more than $\omega^2$. We denote the new, scaled version of $cn(t,m)$ as $J(t,m)$, defined in Appendix B.

Substituting this term into (9), we generate:

$$\ddot{\theta} + \frac{K}{\Omega^2} sign(\dot{\theta}) - \left(\frac{1}{\Omega^2} - \varepsilon \cdot J(t,m)\right)\sin(\theta) = 0 \quad (10),$$

except for the special case where $\dot{\theta} = 0$.

### *5.2 Stability Analysis*

The introduction of a nonlinear damping term explains some very odd behaviors in our inverted pendulum. Perhaps the most surprising of these behaviors was the off-center quasi-stability we saw in the experiments. Whereas the Blackburn model [1] only identifies the symmetric up and down positions as stable fixed points, the inclusion of static friction allows (in fact guarantees) a fixed point off the center. Our normalized static equation is:

$$\ddot{\theta} + \frac{K_S}{\Omega^2} - \left(\frac{1}{\Omega^2} - \varepsilon \cdot J(t,m)\right)\sin(\theta) = 0 \quad (11),$$

where

$$\left|\frac{K_S}{\Omega^2}\right| = \min\left(\frac{F_S}{\Omega^2}, \left|\left(\frac{1}{\Omega^2} - \varepsilon \cdot J(t,m)\right)\sin\theta\right|\right) \quad (12).$$

For all cases where

$$F_S \geq \left|\left(1 - \Omega^2 \varepsilon \cdot J(t,m)\right)\sin\theta\right| \quad (13),$$

the equation is stable. Solving for $\theta$:

$$|\theta| \leq \theta_C = \arcsin\left|\frac{F_S}{1 - \Omega^2 \varepsilon \cdot J(t,m)}\right| \quad (14).$$

So for all nonzero static torques $F_S$, there exist degenerate fixed points in the range $|\theta| \leq \theta_C$, and unless we decay to exactly 0, our oscillations around 0 will cease as soon as they have an

amplitude less than $\theta_C$. This off center stabilization is apparent in Figure 6c, where the experimental results end slightly off center. The model ends at the center, because it does not incorporate static friction (due to the difficulty of pinpointing zero velocity in a linear ODE solver).

The existence of these fixed points has several consequences for our stability model. For parameter values near the boundary of stability, the applied acceleration $1-\Omega^2\varepsilon\cdot J(t,m)$ is minimal, and the deviation of the angle of stability from the center is maximized. As the relative amplitude or frequency of the forcing function is increased, the dynamics go further into the region of stability, and $\theta_C$ approaches 0. This evolution of the phase space matches our empirical observations.

The lack of noticeable dependency on *m* in Figure 7b is easily understood by looking at Figure 10. Even an eccentricity as large as 0.9999 – far beyond our experimental range – results in an essentially sinusoidal displacement. So as long as we are in the displacement domain, we see little dependence on *m*. If we use maximum acceleration as a parameter (as in Figure 6a), then the amplitude scaling $\rho(m)$ (from Appendix B) exactly accounts for the dependency on *m*.

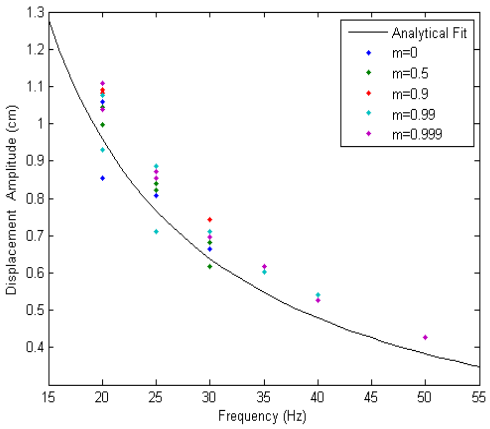


**Figure 8.** Experimental versus analytically derived boundary of stability. The analytical fit is from(20), $a\omega = \sqrt{2gr^*}$. Discrepancies between the analytical and experimental results could be due to noisy measurement mentioned in Section 3.3. Additionally, there may be some small dependency on *m* that the analysis did not take into consideration. This may account for why the low *m* track better to the curve than the high *m*.

Both the numerical and experimental results showed stability dependent on the product of the amplitude and frequency of the forcing function. This boundary can be derived analytically, with some simplifying assumptions. We will set $\theta \approx \sin\theta$, use (3) as our forcing function, and drop the frictional torque. Our system is now

$$I\ddot{\theta} - Mrg\theta = -Mra\omega^2\cos(\omega t)\theta \quad (15).$$

At the boundary of stability the forcing function counteracts gravity sufficiently that we have an unstable limit cycle with period $2\pi/\omega$. By double integrating the right side of (15) we generate a first pass deterministic approximation for $\theta(t)$ of:

$$\theta(t) = \theta_0 + \left(\frac{a}{r^*}\cos(\omega t)\right)\sin\theta = \theta_0\left(1+\frac{a}{r^*}\cos(\omega t)\right) \quad (16).$$

Plugging this back into (15) we get:

$$I\ddot{\theta} = Mrg\theta_0\left(1-\frac{a\omega^2}{g}\cos(\omega t)\right)\left(1+\frac{a}{r^*}\cos(\omega t)\right) \quad (17).$$

The unstable limit cycle exists when the double integral over the period – the change in location after one period of the forcing function – is zero. If $\Delta\theta/\theta<0$, then the pendulum will eventually stabilize at $\theta = 0$. If $\Delta\theta/\theta>0$, the pendulum will eventually fall away from the inverted position. Therefore the equality $0 = \Delta\theta = \iint_T \ddot{\theta}dt^2$ is true at the boundary of stability. This expands to:

$$0 = \frac{\Delta\theta}{\theta_0} = \iint_T\left(1-\frac{a\omega^2}{g}\cos(\omega t)\right)\left(1+\frac{a}{r^*}\cos(\omega t)\right)dt^2 \quad (18).$$

Integrating, we get:

$$0 = \frac{T^2}{2}\left(1-\frac{a^2\omega^2}{2gr^*}\right) \quad (19),$$

which solves to :

$$a\omega = \sqrt{2gr^*} \quad (20).$$

This curve maps well to our data, as can be seen in Figure 8. If we convert to relative amplitude and frequency, (20) becomes:

$$\varepsilon\Omega = \sqrt{2} \quad (21),$$

which exactly corresponds to the boundary of stability found by Blackburn et al. in Figure 1.

Both the numerical and experimental results showed stability dependent on the product of the amplitude and frequency of the forcing function. This boundary can be derived analytically, with some simplifying assumptions. We will set $\theta \approx \sin\theta$, use (3) as our forcing function, and drop the frictional torque. Our system is now

$$I\ddot{\theta} - Mrg\theta = -Mra\omega^2\cos(\omega t)\theta \quad (15).$$

At the boundary of stability the forcing function counteracts gravity sufficiently that we have an unstable limit cycle with period $2\pi/\omega$. By double integrating the right side of (15) we generate a first pass deterministic approximation for $\theta(t)$ of:

$$\theta(t) = \theta_0 + \left(\frac{a}{r^*}\cos(\omega t)\right)\sin\theta = \theta_0\left(1+\frac{a}{r^*}\cos(\omega t)\right) \quad (16).$$

Plugging this back into (15) we get:

$$I\ddot{\theta} = Mrg\theta_0\left(1-\frac{a\omega^2}{g}\cos(\omega t)\right)\left(1+\frac{a}{r^*}\cos(\omega t)\right) \quad (17).$$

The unstable limit cycle exists when the double integral over the period – the change in location after one period of the forcing function – is zero. If $\Delta\theta/\theta<0$, then the pendulum will eventually stabilize at $\theta = 0$. If $\Delta\theta/\theta>0$, the pendulum will eventually fall away from the inverted position. Therefore the equality $0 = \Delta\theta = \iint_T \ddot{\theta}dt^2$ is true at the boundary of stability. This expands to:

$$0 = \frac{\Delta\theta}{\theta_0} = \iint_T\left(1-\frac{a\omega^2}{g}\cos(\omega t)\right)\left(1+\frac{a}{r^*}\cos(\omega t)\right)dt^2 \quad (18).$$

Integrating, we get:

$$0 = \frac{T^2}{2}\left(1-\frac{a^2\omega^2}{2gr^*}\right) \quad (19),$$

which solves to :

$$a\omega = \sqrt{2gr^*} \quad (20).$$

This curve maps well to our data, as can be seen in Figure 8. If we convert to relative amplitude and frequency, (20) becomes:

$$\varepsilon\Omega = \sqrt{2} \quad (21),$$

which exactly corresponds to the boundary of stability found by Blackburn et al. in Figure 1.

## 6. Conclusion

We were able to successfully determine the boundary of stability for an inverted pendulum, both numerically and experimentally. We extended the traditional parameter space of the inverted pendulum by using a Jacobi Elliptical forcing function with scalable eccentricity. While we expected that this would increase the region of stability, we found no measureable effect of forcing eccentricity on the boundary of stability.

We did find analytical justification for the shape of the boundary of stability. Inclusion of friction in our model was vital for understanding the non-exponential decay and off-center stabilization that we observed.

One valuable addition to our research would have been an estimation of the basin of attraction for the stable fixed points. An inability to fix the position and angular velocity during operation rendered such a study infeasible, but perhaps such an apparatus could be built in a future experiment.

## 7. Acknowledgements

We would like to thank Andrei Savu for his assistance in assembling and reassembling the inverted pendulum. Nick Gravish wrote the Labview program that controlled the high speed camera and recorded our movies, and provided invaluable debugging help.

Both Andrei and Nick were graduate students in Professor Dan Goldman's CRAB Lab at Georgia Tech. Professor Goldman also deserves thanks for his assistance and advice in getting the experiments started.

Finally we would like to thank Professor Paul Umbanhowar, who constructed the shaker table and wrote the original controller program.

## Appendix A. Jacobi Elliptical Functions

The Jacobi elliptical function $cn(u,m)$ is defined as follows: Let

$$u = \int_0^{\phi} \frac{d\theta}{\sqrt{1 - m\sin^2\theta}} \quad \text{(A.1)},$$

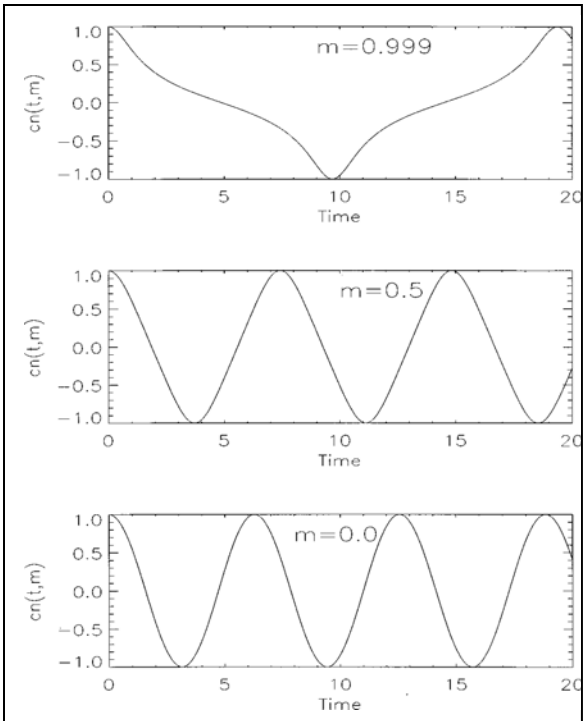


**Figure 9.** Jacobi elliptical cosine $cn(t,m)$ for various values of m [9]. The period increases monotonically with $m$.

then $cn(u,m) = \cos\phi$. The eccentricity parameter $m$ is bounded from 0 to 1. At the limits of $m$, $cn(u,0) = \cos(u)$, and $cn(u,1) = \mathrm{sech}(u)$. For $m > 0$, the period will necessarily be longer than $2\pi$. The period T is defined by the Elliptic Integral,

$$T = K(m) = 4\int_0^{\pi/2} \frac{dt}{\sqrt{1 - m\sin^2 t}} \quad \text{(A.2)}.$$

Figure 9 displays the waveform of $cn(t.m)$ for several values of $m$.

## Appendix B. Scaled Elliptical Function

Our experiment assumes the relative frequency Ω, relative displacement €, and eccentricity of the Jacobi Elliptical to be independent parameters. In order for this to hold true in our model, we must scale the Jacobi Elliptical forcing function so that $J(t,m)$ provides a consistent displacement amplitude of 1 and a consistent period of $2\pi$ for all valid values of $m$.

Scaling the frequency is easily done. Since we already know the period of $cn(t.m)$ is $K(m)$, we

simply scale $t$ by $K(m)/2\pi$ to fix the period to $2\pi$. Scaling the displacement requires numerical double integration of the Jacobi Elliptical at each value of $m$ (an acceleration term) to determine the corresponding amplitude of displacement. After this scaling, we can define

$$J(t,m) = \rho(m)cn(\frac{K(m)}{2\pi}t, m) \quad \text{(B.1)},$$

where

$$\rho(m) = \frac{1}{\int_0^{\pi/2}\int_0^t cn\left(\frac{K(m)}{2\pi}u, m\right)dudt} \quad \text{(B.2)}.$$

Figure 10 shows the Scaled Jacobi Elliptical when $m$ = 0.9999.

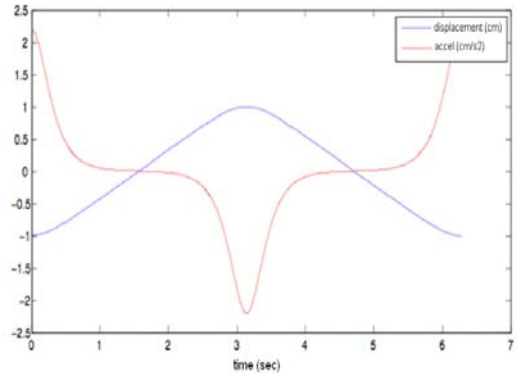


**Figure 10.** Scaled Jacobi Elliptical acceleration and the derived displacement. Even for m as eccentric as 0.9999, the displacement has an amplitude of 1 and a frequency of $2\pi$.

---

***Samuel Shapero*** *is a second year PhD student in the Bioengineering Interdisciplinary Program at Georgia Tech. His research focuses on implementing a sparsity extraction algorithm for high dimensional inputs using nonlinear analog circuits. He has a Master's in Electrical Engineering form Stanford, and has a strong background in analog and digital filter analysis. His research advisor is Dr. Paul Hasler.*

***Yiwei Cheng*** *is a third year PhD student in the School of Civil and Environmental Engineering. Yiwei's main thesis advisor is Dr Marc Stieglitz and his research focuses on understanding how eco-hydrological processes scale. His research focus areas are in the Arctic and Everglades Florida, where he conducts field experiments and simulations.*

***Robert Hayward*** *is a PhD student studying Nuclear and Radiological Engineering at Georgia Tech. He has a Master's in Medical Physics, and has relevant background experience in modeling, numerical methods, and data analysis.*

---

## Works Cited

1. Blackburn, J.A., H.J.T. Smith, and N. Gronbechjensen, Stability and Hopf Bifurcations in an Inverted Pendulum. American Journal of Physics, 1992. 60(10): p. 903-908.
2. Erneux, T. and T. Kalmar-Nagy, Nonlinear stability of a delayed feedback controlled container crane. Journal of Vibration and Control, 2007. 13(5): p. 603-616.
3. Koch, B.P. and R.W. Leven, Subharmonic and Homoclinic Bifurcations in a Parametrically Forced Pendulum. Physica D, 1985. 16(1): p. 1-13.
4. Levi, M. and W. Weckesser, Stabilization of the Inverted Linearized Pendulum by High-Frequency Vibrations. Siam Review, 1995. 37(2): p. 219-223.
5. Mclaughlin, J.B., Period-Doubling Bifurcations and Chaotic Motion for a Parametrically Forced Pendulum. Journal of Statistical Physics, 1981. 24(2): p. 375-388.
6. Milton, J., et al., The time-delayed inverted pendulum: Implications for human balance control. Chaos, 2009. 19(2): p. -.
7. Pathak, K., J. Franch, and S.K. Agrawal, Velocity and position control of a wheeled inverted pendulum by partial feedback linearization. Ieee Transactions on Robotics, 2005. 21(3): p. 505-513.
8. Sanjuan, M.A.F., Subharmonic bifurcations in a pendulum parametrically excited by a non-harmonic perturbation. Chaos Solitons & Fractals, 1998. 9(6): p. 995-1003.
9. Sanjuan, M.A.F., Using nonharmonic forcing to switch the periodicity in nonlinear systems. Physical Review E, 1998. 58(4): p. 4377-4382.
10. Smith, H.J.T. and J.A. Blackburn, Experimental-Study of an Inverted Pendulum. American Journal of Physics, 1992. 60(10): p. 909-911.

Supplemental material, including a picture of the group members and videos of the inverted pendulum in action, can be found at our website invertpend.wordpress.com.